Superradiant Detection of Microscopic Optical Dipolar Interactions

Lingjing Ji,[*,†] Yizun He[●],[*] Qingnan Cai, Zhening Fang[●], Yuzhuo Wang, Liyang Qiu[●], Lei Zhou,[‡] and Saijun Wu[●][§]

*Department of Physics, State Key Laboratory of Surface Physics and Key Laboratory of Micro and
Nano Photonic Structures (Ministry of Education), Fudan University,
Shanghai 200433, China*

Stefano Grava[●][*] and Darrick E. Chang[∥]

*ICFO-Institut de Ciencies Fotoniques, The Barcelona Institute of Science and Technology,
08860 Castelldefels, Barcelona, Spain
and ICREA-Institució Catalana de Recerca i Estudis Avançats, 08015 Barcelona, Spain*

The interaction between light and cold atoms is a complex phenomenon potentially featuring many-body resonant dipole interactions. A major obstacle toward exploring these quantum resources of the system is macroscopic light propagation effects, which not only limit the available time for the microscopic correlations to locally build up, but also create a directional, superradiant emission background whose variations can overwhelm the microscopic effects. In this Letter, we demonstrate a method to perform "background-free" detection of the microscopic optical dynamics in a laser-cooled atomic ensemble. This is made possible by transiently suppressing the macroscopic optical propagation over a substantial time, before a recall of superradiance that imprints the effect of the accumulated microscopic dynamics onto an efficiently detectable outgoing field. We apply this technique to unveil and precisely characterize a density-dependent, microscopic dipolar dephasing effect that generally limits the lifetime of optical spin-wave order in ensemble-based atom-light interfaces.

Interactions between light and atomic ensembles are generically complex phenomena. Even in the weak optical excitation limit, microscopic correlations can build up through resonant dipole interactions and multiple scattering, leading to highly nontrivial anomalous optical response [1–8] or even wave localization [9–15]. For stronger excitations [16–21], the many-body dynamics may start to span the exponentially large Hilbert space and become difficult to understand. Nevertheless, our prevailing theory of quantum light-atom interfaces, the Maxwell-Bloch equations (MBE) [22–27] that largely ignore microscopic correlations, remains highly successful. To experimentally quantify the microscopic correlations, the measurements need to be carefully designed to isolate any effects being well-described by the standard MBE [3–6,15,28,29]. Although methods to elucidate interactions beyond MBE have also been developed in the field of nonlinear optics [30–37], their utility clearly lags behind the level at which microscopic degrees of freedom are controlled and measured in the microwave domain, such as in nuclear magnetic resonance (NMR) [38–43].

Why is there a significant difference between NMR and atom-light interfaces in resolving microscopic correlations? A key answer was provided in a seminal paper more than 70 years ago [44] where Van Vleck suggested that his treatment of many-body spin-relaxation dynamics in NMR may not be applicable to light, due to Doppler and radiation broadening. Indeed, in the optical domain the atomic motion and radiation effectively smooth away and damp out the microscopic correlations. Today, while laser-cooling techniques can freeze out the atomic motion, the collective radiation [45–48] and more generally the propagation of light itself remain an effective damping mechanism to suppress local optical dipolar correlations from freely building up. Furthermore, to resolve the microscopically driven effects from the typically much stronger collective radiation background often requires detailed knowledge of optical propagation for a side-by-side comparison between experimental measurements and numerical modeling [3–6,49].

In this Letter, we probe microscopic correlations in a quantum atom-light interface by completely suppressing the macroscopic light propagation and the associated collective damping of atomic dipoles in free space. The atomic ensemble is laser-cooled to be effectively motionless. The collective damping suppression is achieved by shifting an optically excited spin wave in **k**-space beyond the light cone [48]. This reversible suppression of collective dynamics allows the interaction associated with microscopic dynamics to accumulate over a long "interrogation time" T_i, before a backward **k**-shift to map the effects onto collective radiation for efficient measurement. Importantly,
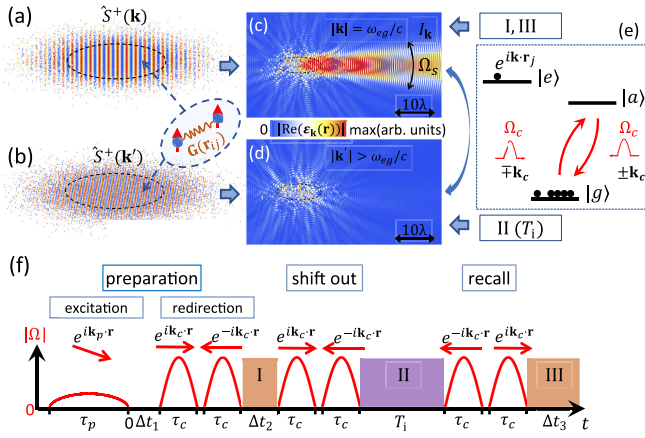
FIG. 1. Probing optical spin wave relaxation in a random gas. (a), (b) illustrate the spin-wave order initiated in a Gaussian distributed random 2-level gas for $|\mathbf{k}| = \omega_{eg}/c$ and $|\mathbf{k}'| = 2.9\omega_{eg}/c$, respectively. The corresponding electric fields $|\mathrm{Re}(\boldsymbol{\varepsilon}_{\mathbf{k}}(\mathbf{r}))|$, calculated over a two-dimensional cut at the sample center, are simulated with the coupled dipole model (CDM) and plotted in (c),(d). See Ref. [51] for details of the simulation. (e) and (f) outline the general spin-wave control scheme and the timing sequence in this work [51], respectively, to unveil microscopic interaction by a reversible suppression of the collective damping with coherent spin-wave control.

the suppression of collective radiation during T_i makes our measurement "background-free," i.e., immune to false signals associated with inaccurate modeling of light propagation itself [3–6,49]. By applying the method to an atomic ensemble, we unveil a fundamental density-dependent dipolar dephasing effect, with a rate that matches precisely with a first-principles theory based on strong near-field optical interactions.

Our experimental method relies on generating and monitoring optical excitations that are free from collective emission. As illustrated in Fig. 1, we consider N 3-level atoms at locations $\{\mathbf{r}_j\}$, $j = 1, \ldots, N$ subjected to a pulsed far-field optical excitation (or a CW excitation that is rapidly switched off). Spin waves associated with the collective raising operator $\hat{S}^+(\mathbf{k}) = 1/\sqrt{N} \sum_j e^{i\mathbf{k}\cdot\mathbf{r}_j} |e_j\rangle\langle g_j|$ can be excited if the wave vector $\mathbf{k}$ of the light satisfies $|\mathbf{k}| = \omega_{eg}/c$, i.e., if the associated frequency is resonant to the atomic transition. Conversely, the same $|\mathbf{k}| = \omega_{eg}/c$ phase-matching condition ensures that the $S^+(\mathbf{k})$ excitation radiates collectively into that light mode. To monitor the spin-wave dynamics, one simply collects the directional emission $I_{\mathbf{k}}(t)$ over a superradiant solid angle Ω_s [45,46,50] [see Fig. 1(c), also see Ref. [51] for rigorous definitions]. The superradiant emission leads to collective damping of the optical excitation with a rate $\Gamma_{\mathbf{k}} \approx [1 + \overline{\mathrm{OD}}(\hat{\mathbf{k}})/4]\Gamma_e$ that can be substantially larger than the natural linewidth Γ_e, where $\overline{\mathrm{OD}}(\hat{\mathbf{k}})$ is the average optical depth of the sample along $\mathbf{k}$ [50].

It is important to note that the collective damping associated with phase-matched radiation exists ubiquitously

in macroscopic optical phenomena and is well described by MBE in continuous media [22]. In fact, the macroscopic control of superradiant emission relies on the associated damping to limit microscopic interaction effects from building up inside quantum interfaces [70]. Here, as we hope to unveil such effects, the collective radiation becomes an enormous background to easily obscure our intended observation. To circumvent the collective damping, we exploit a time-domain phase-matching control technique [48,52] to make rapid and efficient conversion between $S(\mathbf{k})$ and $S(\mathbf{k}')$ spin-wave excitations, with $|\mathbf{k}'| > \omega_{eg}/c$ strongly mismatched from radiation [53]. In absence of collective damping, one expects decay of the optical excitation to be slowed down substantially toward Γ_e [52]. More formally, we define a "survival ratio,"

$$O_{\mathbf{k}'}(t) = |\langle\psi_{\mathbf{k}'}|\psi(t)\rangle|^2, \qquad (1)$$

where the spin-wave state $|\psi(t)\rangle$ is initialized with a singly excited $|\psi_{\mathbf{k}'}\rangle \equiv S^+(\mathbf{k}')|g_1, \ldots, g_N\rangle$ and evolves under the effective non-Hermitian Hamiltonian $H_{\mathrm{eff}} = \sum_{i,j} \hat{V}_{\mathrm{DD}}^{i,j}$ [54,71] with

$$\hat{V}_{\mathrm{DD}}^{i,j} = -\frac{\omega_{eg}^2}{\varepsilon_0 c^2} \mathbf{d}_{ge}^* \cdot \mathbf{G}(\mathbf{r}_{ij}, \omega_{eg}) \cdot \mathbf{d}_{ge}\sigma_i^+\sigma_j^-. \qquad (2)$$

Here, $\sigma_j^- = |g_j\rangle\langle e_j|$ and $\sigma_j^+ = (\sigma_j^-)^\dagger$ are the single-atom spin-lowering and raising operators, respectively, and $\mathbf{d}_{ge}$ is the transition dipole matrix element. The complex symmetric free-space electromagnetic Green's tensor $\mathbf{G}(\mathbf{r}_{ij}, \omega_{eg})$ with $\mathbf{r}_{ij} \equiv \mathbf{r}_i - \mathbf{r}_j$ describes how light propagates from one dipole point source to another. H_{eff} thus encodes both purely coherent interactions, such as those arising from the optical near-field component $\mathbf{G}^{\mathrm{near}}(\mathbf{r}_{ij}) \sim 1/r_{ij}^3$, and collective emission, which arises purely from the far-field, radiating component $\mathbf{G}^{\mathrm{far}}(\mathbf{r}_{ij}) \sim 1/r_{ij}$ and gives H_{eff} its non-Hermitian nature. In the following, we demonstrate that the decay rate $\Gamma_{\mathbf{k}'} = \Gamma_e + \gamma$ for $O_{\mathbf{k}'}(t)$ not only contains a well-known contribution from radiation (Γ_e) [52], but also a dephasing rate $\gamma = C\rho\lambda_{eg}^3$ that depends on the atomic density ρ and arises from $\mathbf{G}^{\mathrm{near}}(\mathbf{r})$, in close analogy to NMR magnetic dipolar relaxation [40,44,72,73].

We follow the control and measurement protocol in Ref. [48] to investigate decay of optical spin-wave order in laser-cooled ^{87}Rb atoms. The spin waves are defined on the $5S_{1/2}, F = 2$ to $5P_{3/2}, F' = 3$ hyperfine transition, with the Zeeman sub-levels labeled as $|g\rangle$ and $|e\rangle$, respectively [Fig. 1(e)]. As in Fig. 1(f), a short probe pulse with wave vector $\mathbf{k}_p$ ($|\mathbf{k}_p| = \omega_{eg}/c$) is applied to resonantly excite the optical spin wave defined on the $|g\rangle - |e\rangle$ transition. We then successively drive population inversions from $|g\rangle \rightarrow |a\rangle$ and back $|a\rangle \rightarrow |g\rangle$ with a pair of pulses on the $5S_{1/2}, F = 2$ to $5P_{1/2}, F'$ D1 transition, with the first and second pulses having wave vectors $\pm\mathbf{k}_c$ and $\mp\mathbf{k}_c$,

respectively [Fig. 1(e)]. Although all atoms initially in $|g\rangle$ wind up back in the same state, the difference in local phases of the pulses seen by each atom causes each to pick up a nontrivial, spatially dependent geometric phase. It can be readily shown [50] that this phase patterning exactly leads to a wave vector shift $\mathbf{k}_p \rightarrow \mathbf{k}_p \mp 2\mathbf{k}_c$ for the spin-wave excitation $S^+(\mathbf{k}_p)$. The control direction $\mathbf{k}_c$ is finely aligned to ensure that the new direction $\mathbf{k} = \mathbf{k}_p - 2\mathbf{k}_c$ is also phase-matched, $|\mathbf{k}| = \omega_{eg}/c$, and thus the spin wave preferentially emits in the $\mathbf{k}$ direction, as illustrated in Fig. 1(c). This has the advantage that the spin-wave population can be read out by the detection of superradiant emission without risking detector saturation by the excitation pulse [45–47,74,75].

After the preparation of the $S^+(\mathbf{k})$ excitation, we investigate the dynamics of phase-mismatched spin waves by immediately applying a second pair of control pulses to shift the spin wave vector to $\mathbf{k}' = \mathbf{k} - 2\mathbf{k}_c$, where $|\mathbf{k}'| = 2.9\omega_{eg}/c$. This large wave vector mismatch from free-space radiation ensures the complete suppression of collective emission for our system sizes $\sigma \gg \lambda$ [53]. After an interrogation time T_i for the $S^+(\mathbf{k}')$ spin wave to accumulate dynamics, a backward shift $\mathbf{k} \rightarrow \mathbf{k} + 2\mathbf{k}_c$ is applied to recall the superradiance [Figs. 1(c) and 1(f)]. The peak amplitude of the exponentially decaying superradiance signal $I_{\mathbf{k}}(t)$ after the recall [interval III in Fig. 1(f)] is proportional to the survival ratio, $\bar{I}_{\mathbf{k}}(T_i) \propto O_{\mathbf{k}'}(T_i)$ defined by Eq. (1) [51]. The decay of $\bar{I}_{\mathbf{k}}(T_i)$ vs T_i therefore directly reveals the decay of phase-mismatched spin waves during the interrogation time.

Experimentally, the ^{87}Rb samples are released from a compressed dipole trap, before being subjected to a weak probe excitation and repeated spin-wave controls [Figs. 1(c) and 1(f)], during which the superradiance $I_{\mathbf{k}}(t)$ is recorded by multimode fiber coupled single photon counters with 0.5 ns temporal resolution [48,50]. The superradiance collection optics has a numerical aperture of NA = 0.06, capable of collecting a substantial fraction of $I_{\mathbf{k}}$ spanning $\Theta \sim \lambda_{eg}/\pi\sigma$ [Fig. 1(c)], even for the most compressed samples with a Gaussian radius $\sigma \approx 3$ μm in this work [Figs. 3(a) and 3(c)] [51]. The detection efficiency for the collected photons is around $Q \sim 0.1$ after all the fiber coupling losses [50,51]. The probe and control pulse durations are $\tau_c = 0.6$ and $\tau_p = 5$ ns, respectively, short enough to uniformly address the dilute samples with negligible absorption and dispersion [51]. The probe pulse area $\theta_p = \int_{-\tau_p}^{0} \Omega_p dt$ is kept below $\pi/10$ with less than 3% population in $|e\rangle$, to ensure the linear excitation criterion [55] so that the dynamics governed by Eq. (2) can be efficiently simulated with a coupled dipole model (CDM) [51,56], and also to avoid saturating the single-photon counters during the superradiant measurements. To investigate the spin-wave dynamics under various conditions, the samples are shaped with different aspect
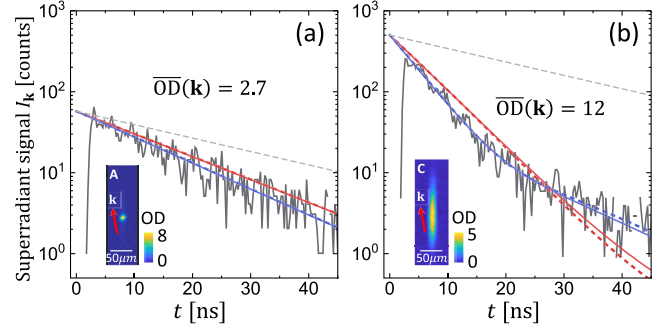

FIG. 2. Superradiant dynamics for phase-matched $S^+(\mathbf{k})$ spin-wave excitation. Time-dependent fluorescence counts are histogrammed into intensity data $I_{\mathbf{k}}(t)$ in (a) and (b). Blue solid (dashed) curves are predictions by CDM (MBE). Red solid (dashed) curves are the expected nearly exponential decay dynamics of the spin wave survival ratio, $O_{\mathbf{k}}(t) \approx e^{-(1+\overline{\text{OD}}(\hat{\mathbf{k}})/4)\Gamma_e t}$ obtained by CDM (MBE) for $|\mathbf{k}| = \omega_{eg}/c$. The gray dashed lines indicate the $e^{-\Gamma_e t}$ spontaneous emission of an isolated atom. The insets are absorption images of the type A, C samples [51]. Red arrows highlight the spin-wave $\mathbf{k}$ direction along which $I_{\mathbf{k}}(t)$ is collected.

ratios initially, see the absorption images in the insets of Figs. 2 and 3, for example. The spherical "A" samples can transiently reach a peak density as high as $\rho_0 \approx 4 \times 10^{13}/\text{cm}^3$. The type "B, C" samples are elongated along z for reaching a high $\overline{\text{OD}}(\hat{\mathbf{k}})$ while maintaining a moderate ρ_0. In addition, the ballistic expansion naturally serves to continuously tune the peak ρ_0 and $\overline{\text{OD}}(\hat{\mathbf{k}})$ parameters, during a 70 μs time-of-flight (TOF) when typically $N_{\text{rep}} = 100$ independent measurements are made for each sample. Data from these repeated measurements are grouped according to the sequence parameters and estimated density distributions, to average and enhance the $I_{\mathbf{k}}(t)$ signals for the following analysis [51].

We first investigate dynamics of superradiant emission associated with the phase-matched $S^+(\mathbf{k})$ spin wave. For this purpose, the atoms are allowed to evolve freely after the $S^+(\mathbf{k})$ spin-wave preparation [The "I" interval in Fig. 1(f) with long enough Δt_2.]. Typical $I_{\mathbf{k}}(t)$ are given in Figs. 2(a) and 2(b) collected from type A,C samples over the same number of measurement repetitions under otherwise nearly identical experimental conditions [51]. The relative amplitudes of the superradiance signals are therefore decided by the atomic number N and the optical depth $\overline{\text{OD}}$ [50]. It is known that the $I_{\mathbf{k}}(t)$ superradiance signal deviates from the decay of the spin wave itself as a result of small-angle diffraction that reshapes the superradiance profile [50,57]. The reshaping effect generally leads to a rapid initial decay of $I_{\mathbf{k}}(t)$, beyond the $[1 + \overline{\text{OD}}(\mathbf{k})/4]\Gamma_e$ rate for $O_{\mathbf{k}}(t)$, followed by a nonexponential tail. The accuracy of the $I_{\mathbf{k}}$ measurements is confirmed by both CDM and MBE simulations that reproduce the nontrivial collective dynamics, with *no freely adjustable parameters* [51]. The tiny
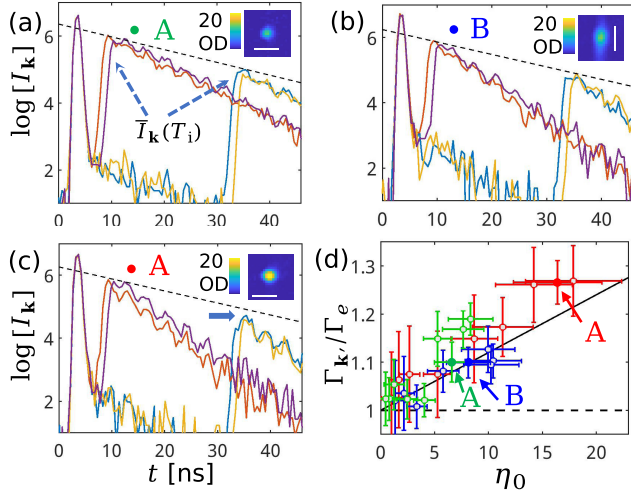
FIG. 3. Decay of the $|\mathbf{k}'| \neq \omega_{eg}/c$ spin wave. (a)–(c): Superradiance $I_{\mathbf{k}}(t)$ during the full control sequence [Fig. 1(f)] with $T_{\mathrm{i}} = [1.2, 2.5, 25.8, 27.0]$ ns (red, purple, blue, and yellow curves), for three typical, fairly dense samples. Exponential fits to the recalled $I_{\mathbf{k}}(t)$ curves leads to $\Gamma_{\mathbf{k}} \approx \{1.9, 2.8, 3.2\}\Gamma_e$ for (a)–(c) respectively. A black dashed line with $-\Gamma_e$ slope is added as a reference to compare with the peak $\bar{I}_{\mathbf{k}}(T_{\mathrm{i}})$ decay. Substantial deviation of $I_{\mathbf{k}}(T_{\mathrm{i}})$ from the MBE-predicted line is highlighted with an arrow in (c). The atomic distribution is inferred from strong-exposure absorption images [51], as in the insets (white scale bar = 20 μm). (d) The $\Gamma_{\mathbf{k}'}$ estimated from the four $\bar{I}_{\mathbf{k}}(T_{\mathrm{i}})$ peaks [51] is plotted vs the estimated dimensionless peak density parameter $\eta_0 = \rho_0 \lambda_{eg}^3$ in different colors. The y-error bars reflect the statistical and systematic uncertainties. The x-error bars $\Delta\eta_0 = \pm 25\%\eta_0$ are associated with uncertainties in the sample preparation and characterization. The solid black line gives the prediction from the dipolar dephasing theory of Eq. (3), with $\bar{\eta} = \eta_0/2\sqrt{2}$ as the mean density of a Gaussian distribution. The horizontal dashed line, $\Gamma_{\mathbf{k}'} = \Gamma_e$, based on MBE, ignores microscopic effects associated with atomic granularity.

difference between the CDM and MBE predictions, originating from the microscopic interaction captured by CDM, is hardly visible in Fig. 2 and impossible to distinguish through the $I_{\mathbf{k}}(t)$ measurements in presence of such collective dynamics background.

To unveil the microscopic dephasing dynamics predicted by CDM, we now proceed with the full spin-wave control sequence [Fig. 1(f)]. Typical $I_{\mathbf{k}}(t)$ with interrogation times $T_{\mathrm{i}} = [1.2, 2.5, 25.8, 27.0]$ ns are plotted in Figs. 3(a)–3(c) with colored curves. As detailed in Ref. [51], this timing suppresses a systematic bias to the spin-wave recall efficiency due to a T_{i}-dependent hyperfine interference effect [50]. The samples are from the initial TOF with negligible expansion [51]. At each T_{i}, the signal $I_{\mathbf{k}}(t)$ has two peaks. The first peak corresponds to the interval I in Fig. 1(f), and arises immediately following the preparation of the spin wave $S^+(\mathbf{k})$. The signal then effectively vanishes once the second pair of control pulses is applied to shift the spin wave to a phase-mismatched $S^+(\mathbf{k}')$,

remains for T_{i}, until it is recalled back to $S^+(\mathbf{k})$ to produce the second superradiance peak (interval III). Not surprisingly, once the spin wave is recalled back to the phase-matched state, the intensity $I_{\mathbf{k}}(t)$ decays at a superradiant rate enhanced by $\overline{\mathrm{OD}}(\mathbf{k})$, similar to the Fig. 2 data. More important, however, is the decay of the recalled amplitude peaks $\bar{I}_{\mathbf{k}}(T_{\mathrm{i}})$, which, with the precise timing knowledge [48,51], are retrieved by fitting the recalled $I_{\mathbf{k}}(t)$ with exponentials in interval III [Fig. 1(f)].

We now examine the decay of $\bar{I}_{\mathbf{k}}(T_{\mathrm{i}})$ vs T_{i} in Figs. 3(a)–3(c) for possible deviation from the single atom rate Γ_e [52] prescribed by MBE (dashed black lines). The deviation is hardly seen in Fig. 3(a) type A samples with reduced $N \approx 8 \times 10^3$, but becomes apparent when the atom number is increased to $N \approx 2 \times 10^4$ in Fig. 3(c) so that $\rho_0 \approx 4 \times 10^{13}/\mathrm{cm}^3$ is reached. Notice both the Figs. 3(a) and 3(c) samples are during their initial TOF with essentially identical spatial distributions [51]. On the other hand, for the elongated B samples in Fig. 3(b), the deviation is substantially reduced, due to the smaller density, even though the recalled $I_{\mathbf{k}}(t)$ decays almost as rapidly as those in Fig. 3(c). Similar observation is made for the type C samples [Fig. 2(b)] with even larger OD. For all the measurements, we fit the $\{\bar{I}_{\mathbf{k}}(T_{\mathrm{i}}), T_{\mathrm{i}}\}$ data according to $\bar{I}_{\mathbf{k}}(T_{\mathrm{i}}) \propto O_{\mathbf{k}'}(T_{\mathrm{i}}) = e^{-\Gamma_{\mathbf{k}'} T_{\mathrm{i}}}$. The decay rates $\Gamma_{\mathbf{k}'}$ are plotted in Fig. 3(d) vs the corresponding dimensionless density parameter $\eta_0 = \rho_0 \lambda_{eg}^3$. From Fig. 3(d), a density-dependent dephasing rate $\gamma \approx 0.013(3)\eta_0 \Gamma_e$ can be extracted.

The density-dependent deviation of $\Gamma_{\mathbf{k}'}$ from the MBE-predicted rate Γ_e in Fig. 3(d) is our main measurement result. The additional decay may not be a complete surprise [52], since the spin-wave state $|\psi_{\mathbf{k}'}\rangle$ is not an eigenstate of H_{eff} by Eq. (2) for a random gas. In the following we clarify that the $1/r^3$ scaling of the near-field interaction in Eq. (2) determines the exponential form of the additional spin-wave decay. We then provide an analytical expression of γ to be compared with the measurement. We focus on the initial spin-wave dynamics within $\delta t \ll 1/\Gamma_e$, where the effects by the anti-Hermitian part H_{a} associated with far-field radiation can be separated from the Hermitian part H_{r} of $H_{\mathrm{eff}} = H_{\mathrm{a}} + H_{\mathrm{r}}$ (see Sec. S1A of Ref. [51]). The impact of dephasing to $O_{\mathbf{k}'}(\delta t)$ is formally captured by considering the decomposition of $|\psi_{\mathbf{k}'}\rangle$ in the eigenstate basis of H_{r}, $\{|n\rangle\}$, and evaluating the spectrum $P(\omega) \equiv \sum_n |\langle n|\psi_{\mathbf{k}'}\rangle|^2 \delta(\omega - \omega_n)$ [76]. In order to arrive at a simple effective theory, the key realization is that in a random gas and for the resonant dipole interaction of Eq. (2), the high-frequency tails of $P(\omega)$ are governed not by the entire many-atom system, but only by a small fraction of atomic pairs with separations $r \ll \lambda_{eg}/2\pi$. This results in strong frequency shifts of each pair due to near-field interactions $\omega_n \propto 1/r^3$, which dominate over the interactions of the pair with all other atoms combined [58]. As detailed in Ref. [51], these pairwise interactions yield a $P(\omega) \propto 1/\omega^2$

large-frequency scaling in a random gas [59]. Its Fourier transform leads to an initial decay of $O_{\mathbf{k}'}(\delta t) = e^{-(\Gamma_e + \gamma)\delta t}$, with

$$\gamma = \xi\eta\Gamma_e. \tag{3}$$

Here $\eta = \rho\lambda_{eg}^3$ is the dimensionless density, while ξ is a numerical factor that depends on details of the dipolar interaction. Beyond the 2-level model, in Ref. [51] we derive the value of ξ for various models including those taking into account hyperfine interactions. In particular, $\xi = 0.64/6\pi$ for the $F = 2 - F' = 3$ transition of ^{87}Rb. We further account for the fact that the atomic ensemble has a Gaussian rather than uniform density distribution. Defining $\bar{\eta} = \eta_0/2\sqrt{2}$ as the mean density, one can show that the dephasing rate becomes $\Gamma_{\mathbf{k}'} = \Gamma_e(1 + \xi\bar{\eta})$ for the Gaussian distribution. In Fig. 3(d) we see excellent agreement between the experimental measurements with this model which suggests $\gamma = 0.012\eta_0\Gamma_e$. We refer readers to Refs. [51,53] for a general discussion on the long-term behavior of the survival ratio beyond the initial decay.

The near-field relaxation mechanism shares the same physics origin with that regularly observed in NMR, where similar line shape analyses were made in frequency and time domain spectroscopy [40,44,72,77,78]. Here, for atom-light interactions, the observation is made possible by suppressing the collective radiation damping which becomes significant in the optical domain [44]. We expect similar dephasing effects arise in solid-state ensembles, such as rare-earth doped systems [79,80] with typically orders-of-magnitude larger emitter densities. Importantly, for a macroscopic sample with size $L \gg \lambda_{eg}$, the collective dynamics associated with $\Gamma_{\mathbf{k}} \sim \overline{\mathrm{OD}}(\mathbf{k})\Gamma_e$ is stronger than the typical microscopic rate $\gamma \sim \bar{\eta}\Gamma_e$ by a factor of L/λ_{eg}. The transient suppression of the collective dynamics background is thus essential for accurate measurements of the microscopic interactions in the far field. We note that similar suppression of light propagation can be achieved by controlling the electromagnetic environment, for example, by periodically dressing a slow-light medium [81–83].

By measuring superradiance following a transient suppression of light propagation, we identify and quantify a density-dependent dephasing effect arising from the near-field optical dipolar interaction. This dephasing effect is universal in dense atomic ensembles [1,7,84–86]. Straightforward extension of our observation to atomic gases near degeneracy would help to uncover spin-dependent correlations related to quantum statistics [1–3,87,88]. To overcome the dephasing effect one might resort to atomic arrays [89] where the fluctuations of near-field interactions are controlled [90,91]. The suppression of collective radiation brings an atom-light interface closer to its NMR counterpart in terms of controllable microscopic interactions. After more than 70 years since the first observation was made in the microwave

domain [44,72,77,78], we hope that the observation of optical dipolar spin-wave relaxation will contribute to novel developments of many-body physics in quantum optics [3,12,14,15,87,88,90–95].

---

[*]These authors contributed equally to this work.
[†]ljji17@fudan.edu.cn
[‡]phzhou@fudan.edu.cn
[§]saijunwu@fudan.edu.cn
[‖]darrick.chang@icfo.eu

[1] O. Morice, Y. Castin, and J. Dalibard, Phys. Rev. A **51**, 3896 (1995).
[2] J. Ruostekoski and J. Javanainen, Phys. Rev. Lett. **82**, 4741 (1999).
[3] P. C. Bons, R. De Haas, D. De Jong, A. Groot, and P. Van Der Straten, Phys. Rev. Lett. **116**, 173602 (2016).
[4] S. Jennewein, M. Besbes, N. J. Schilder, S. D. Jenkins, C. Sauvan, J. Ruostekoski, J.-J. Greffet, Y. R. P. Sortais, and A. Browaeys, Phys. Rev. Lett. **116**, 233601 (2016).
[5] S. Jennewein, L. Brossard, Y. R. P. Sortais, A. Browaeys, P. Cheinet, J. Robert, and P. Pillet, Phys. Rev. A **97**, 053816 (2018).
[6] S. D. Jenkins, J. Ruostekoski, J. Javanainen, S. Jennewein, R. Bourgain, J. Pellegrino, Y. R. P. Sortais, and A. Browaeys, Phys. Rev. A **94**, 023842 (2016).
[7] N. J. Schilder, C. Sauvan, Y. R. P. Sortais, A. Browaeys, and J. Greffet, Phys. Rev. Lett. **124**, 073403 (2020).
[8] Z. Shen and A. Dogariu, Nat. Photonics **16**, 148 (2022).
[9] G. Labeyrie, F. D. Tomasi, J. C. Bernard, C. A. Müller, C. Miniatura, and R. Kaiser, Phys. Rev. Lett. **83**, 5266 (1999).
[10] Y. Bidel, B. Klappauf, J. C. Bernard, D. Delande, G. Labeyrie, C. Miniatura, D. Wilkowski, and R. Kaiser, Phys. Rev. Lett. **88**, 203902 (2002).
[11] C. M. Aegerter and G. Maret, Prog. Opt. **52**, 1 (2009).

[12] S. E. Skipetrov and I. M. Sokolov, Phys. Rev. Lett. **112,** 023905 (2014).

[13] T. Sperling, L. Schertel, M. Ackermann, G. J. Aubry, C. M. Aegerter, and G. Maret, New J. Phys. **18,** 013039 (2016).

[14] S. E. Skipetrov, Phys. Rev. Lett. **121,** 093601 (2018).

[15] F. Cottier, A. Cipris, R. Bachelard, and R. Kaiser, Phys. Rev. Lett. **123,** 083401 (2019).

[16] Y.-X. Zhang and K. Mølmer, Phys. Rev. Lett. **122,** 203605 (2019).

[17] L. Henriet, J. S. Douglas, D. E. Chang, and A. Albrecht, Phys. Rev. A **99,** 023802 (2019).

[18] L. A. Williamson, M. O. Borgh, and J. Ruostekoski, Phys. Rev. Lett. **125,** 073602 (2020).

[19] S. J. Masson, I. Ferrier-barbut, L. A. Orozco, A. Browaeys, and A. Asenjo-garcia, Phys. Rev. Lett. **125,** 263601 (2020).

[20] L. A. Williamson and J. Ruostekoski, Phys. Rev. Res. **2,** 023273 (2020).

[21] R. J. Bettles, M. D. Lee, S. A. Gardiner, and J. Ruostekoski, Commun. Phys. **3,** 141 (2020).

[22] Y. R. Shen, *The Principles of Nonlinear Optics* (Wiley-Interscience, New York, 2002).

[23] C. M. Bowden and J. P. Dowling, Phys. Rev. A **47,** 1247 (1993).

[24] Y. Castin and K. Molmer, Phys. Rev. A **51,** R3426 (1995).

[25] M. Fleischhauer and S. F. Yelin, Phys. Rev. A **59,** 2427 (1999).

[26] K. Hammerer, A. S. Sørensen, and E. S. Polzik, Rev. Mod. Phys. **82,** 1041 (2010).

[27] A. A. Svidzinsky, X. Zhang, and M. O. Scully, Phys. Rev. A **92,** 013801 (2015).

[28] C. C. Kwong, T. Wellens, K. Pandey, and D. Wilkowski, Phys. Rev. A **102,** 063722 (2020).

[29] M. Maiwöger, M. Sonnleitner, T. Zhang, I. Mazets, M. Mallweger, D. Rätzel, F. Borselli, S. Erne, J. Schmiedmayer, and P. Haslinger, Phys. Rev. X **12,** 031018 (2022).

[30] L. Yang and S. Mukamel, Phys. Rev. Lett. **100,** 057402 (2008).

[31] K. W. Stone, K. Gundogdu, D. B. Turner, X. Li, S. T. Cundiff, and K. A. Nelson, Science **324,** 1169 (2009).

[32] X. Dai, M. Richter, H. Li, A. D. Bristow, C. Falvo, S. Mukamel, and S. T. Cundiff, Phys. Rev. Lett. **108,** 193201 (2012).

[33] H. Li, A. D. Bristow, M. E. Siemens, G. Moody, and S. T. Cundiff, Nat. Commun. **4,** 1390 (2013).

[34] G. Nardin, G. Moody, R. Singh, T. M. Autry, H. Li, F. Morier-Genoud, and S. T. Cundiff, Phys. Rev. Lett. **112,** 046402 (2014).

[35] B. Lomsadze and S. T. Cundiff, Phys. Rev. Lett. **120,** 233401 (2018).

[36] S. Yu, M. Titze, Y. Zhu, X. Liu, and H. Li, Opt. Express **27,** 28891 (2018).

[37] D. Liang, L. S. Rodriguez, H. Zhou, Y. Zhu, and H. Li, Opt. Lett. **47,** 6452 (2022).

[38] P. R. Zangara and H. M. Pastawski, Phys. Scr. **92,** 033001 (2017).

[39] J. Li, R. Fan, H. Wang, B. Ye, B. Zeng, H. Zhai, X. Peng, and J. Du, Phys. Rev. X **7,** 031011 (2017).

[40] G. A. Starkov and B. V. Fine, Phys. Rev. B **101,** 024428 (2020).

[41] C. Brif, R. Chakrabarti, and H. Rabitz, New J. Phys. **12,** 075008 (2010).

[42] J. A. Jones, Prog. Nucl. Magn. Reson. Spectrosc. **59,** 91 (2011).

[43] K. Inomata, A. Ohno, H. Tochio, S. Isogai, T. Tenno, I. Nakase, T. Takeuchi, S. Futaki, Y. Ito, H. Hiroaki, and M. Shirakawa, Nature (London) **458,** 106 (2009).

[44] J. V. Vleck, Phys. Rev. **74,** 1168 (1948).

[45] M. O. Araujo, I. Kresic, R. Kaiser, and W. Guerin, Phys. Rev. Lett. **117,** 073002 (2016).

[46] S. J. Roof, K. J. Kemp, M. D. Havey, and I. M. Sokolov, Phys. Rev. Lett. **117,** 073003 (2016).

[47] S. L. Bromley, B. Zhu, M. Bishof, X. Zhang, T. Bothwell, J. Schachenmayer, T. L. Nicholson, R. Kaiser, S. F. Yelin, M. D. Lukin, A. M. Rey, and J. Ye, Nat. Commun. **7,** 11039 (2016).

[48] Y. He, L. Ji, Y. Wang, L. Qiu, J. Zhao, Y. Ma, X. Huang, S. Wu, and D. E. Chang, Phys. Rev. Lett. **125,** 213602 (2020).

[49] J. Javanainen and J. Ruostekoski, Opt. Express **24,** 993 (2016).

[50] Y. He, L. Ji, Y. Wang, L. Qiu, J. Zhao, Y. Ma, X. Huang, S. Wu, and D. E. Chang, Phys. Rev. Res. **2,** 043418 (2020).

[51] See Supplemental Material at http://link.aps.org/supplemental/10.1103/PhysRevLett.131.253602, which includes Refs. [22,47–50,52–69], for details of theoretical derivation, experimental setup, and data analysis.

[52] M. O. Scully, Phys. Rev. Lett. **115,** 243602 (2015).

[53] S. Grava, Y. He, S. Wu, and D. E. Chang, New J. Phys. **24,** 013031 (2022).

[54] L. Chomaz, L. Corman, T. Yefsah, R. Desbuquois, and J. Dalibard, New J. Phys. **14,** 055001 (2012).

[55] S. Prasad and R. J. Glauber, Phys. Rev. A **82,** 063805 (2010).

[56] B. Zhu, J. Cooper, J. Ye, and A. M. Rey, Phys. Rev. A **94,** 023612 (2016).

[57] F. Cottier, R. Kaiser, and R. Bachelard, Phys. Rev. A **98,** 013622 (2018).

[58] F. Andreoli, M. J. Gullans, A. A. High, A. Browaeys, and D. E. Chang, Phys. Rev. X **11,** 011026 (2021).

[59] L. Bellando, A. Gero, E. Akkermans, and R. Kaiser, Phys. Rev. A **90,** 063822 (2014).

[60] M. Suzuki, Commun. Math. Phys. **51,** 183 (1976).

[61] D. J. Daley and D. Vere-Jones *An introduction to the theory of point processes, volume 1: Elementary theory and methods* (Springer-Verlag, New York, Berlin, Heidelberg, 2003).

[62] E. Munro, A. Asenjo-Garcia, Y. Lin, L. C. Kwek, C. A. Regal, and D. E. Chang, Phys. Rev. A **98,** 033815 (2018).

[63] H. T. Dung, L. Knöll, and D.-G. Welsch, Phys. Rev. A **66,** 063810 (2002).

[64] A. Asenjo-Garcia, M. Moreno-Cardoner, A. Albrecht, H. J. Kimble, and D. E. Chang, Phys. Rev. X **7,** 031024 (2017).

[65] G. Reinaudi, T. Lahaye, Z. Wang, and D. Guéry-Odelin, Opt. Lett. **32,** 3143 (2007).

[66] D. A. Steck, Rubidium 87D Line Data (2003), http://steck.us/alkalidata.

[67] M. O. Scully, E. S. Fry, C. H. R. Ooi, and K. Wódkiewicz, Phys. Rev. Lett. **96,** 010501 (2006).

[68] Y. Ma, R. Liu, L. Ji, L. Qiu, D. Su, Y. Zhao, N. Yao, W. Fang, and S. Wu, Phys. Rev. Appl. **20,** 024041 (2023).

[69] Y. Ma, X. Huang, X. Wang, L. Ji, Y. He, L. Qiu, J. Zhao, Y. Wang, and S. Wu, Opt. Express **28**, 17171 (2020).

[70] L. Duan, M. D. Lukin, J. I. Cirac, and P. Zoller, Nature (London) **414**, 413 (2001).

[71] M. Gross and S. Haroche, Phys. Rep. **93**, 301 (1982).

[72] N. Bloembergen, E. M. Purcell, and R. V. Pound, Phys. Rev. **73**, 679 (1948).

[73] W. Derbyshire, M. Van Den Bosch, D. Van Dusschoten, W. MacNaughtan, I. A. Farhat, M. A. Hemminga, and J. R. Mitchell, J. Magn. Reson. **168**, 278 (2004).

[74] C. C. Kwong, T. Yang, M. S. Pramod, K. Pandey, D. Delande, R. Pierrat, and D. Wilkowski, Phys. Rev. Lett. **113**, 223601 (2014).

[75] S. Zhang, C. Liu, S. Zhou, C. S. Chuu, M. M. Loy, and S. Du, Phys. Rev. Lett. **109**, 1 (2012).

[76] E. J. Heller, in *Chaos and Quantum Physics*, edited by A. Voros and M.-J. Giannoni (North Holland, Amsterdam, 1990).

[77] C. Kittel and E. Abrahams, Phys. Rev. **90**, 238 (1953).

[78] I. J. Lowe and R. E. Norberg, Phys. Rev. **107**, 46 (1957).

[79] M. Zhong, M. P. Hedges, R. L. Ahlefeldt, J. G. Bartholomew, S. E. Beavan, S. M. Wittig, J. J. Longdell, and M. J. Sellars, Nature (London) **517**, 177 (2015).

[80] T. Zhong, J. M. Kindem, E. Miyazono, and A. Faraon, Nat. Commun. **6**, 8206 (2015).

[81] M. Bajcsy, A. S. Zibrov, and M. D. Lukin, Nature (London) **426**, 638 (2003).

[82] A. André, M. Bajcsy, A. S. Zibrov, and M. D. Lukin, Phys. Rev. Lett. **94**, 063902 (2005).

[83] K. K. Park, Y. W. Cho, Y. T. Chough, and Y. H. Kim, Phys. Rev. X **8**, 021016 (2018).

[84] Yu. N. Barabanenkov and V. V. Shlyapin, Phys. Lett. A **170**, 239 (1992).

[85] J. Javanainen, J. Ruostekoski, Y. Li, and S.-M. Yoo, Phys. Rev. A **96**, 033835 (2017).

[86] A. Cipris, R. Bachelard, R. Kaiser, and W. Guerin, Phys. Rev. A **103**, 033714 (2021).

[87] A. B. Deb and N. Kjærgaard, Science **374**, 972 (2021).

[88] Y. K. Lu, Y. Margalit, and W. Ketterle, Nat. Phys. **19**, 210 (2022).

[89] G. Facchinetti, S. D. Jenkins, and J. Ruostekoski, Phys. Rev. Lett. **117**, 243601 (2016).

[90] J. Rui, D. Wei, A. Rubio-abadal, S. Hollerith, D. M. Stamper-kurn, C. Gross, and I. Bloch, Nature (London) **583**, 369 (2020).

[91] K. Srakaew, P. Weckesser, S. Hollerith, D. Wei, D. Adler, I. Bloch, and J. Zeiher, Nat. Phys. **10**, 1038 (2023).

[92] N. Y. Yao, C. R. Laumann, S. Gopalakrishnan, M. Knap, M. Müller, E. A. Demler, and M. D. Lukin, Phys. Rev. Lett. **113**, 243002 (2014).

[93] L. F. Santos, F. Borgonovi, and G. L. Celardo, Phys. Rev. Lett. **116**, 250402 (2016).

[94] C. C. Rusconi, T. Shi, and J. I. Cirac, Phys. Rev. A **104**, 033718 (2021).

[95] T. Bilitewski, A. P. Orioli, C. Sanner, L. Sonderhouse, R. B. Hutson, L. Yan, W. R. Milner, J. Ye, and A. M. Rey, Phys. Rev. Lett. **128**, 093001 (2022).